Zentrum für Technomathematik

Fachbereich 3 – Mathematik und Informatik

Adaptivity in 3D Image Processing

Eberhard Bänsch **Karol Mikula**

Report 99–14

Berichte aus der Technomathematik

Report 99–14 **Dezember 1999**

Adaptivity in 3D Image Processing

Eberhard Bänsch* Karol Mikula†

Abstract. We present an adaptive numerical scheme for computing the nonlinear partial differential equations arising in 3D image multiscale analysis. The scheme is based on a semi-implicit scale discretization and on an adaptive finite element method in 3D-space. Successive coarsening of the computational grid is used for increasing the efficiency of the numerical procedure. L_∞-stability of the suggested numerical method is presented and computational results related to 3D nonlinear image filtering are discussed.

Key words: nonlinear diffusion equations, numerical solution, finite element method, unstructured grids, image processing, anisotropic diffusion, image smoothing.

AMS(MOS) subject classifications: 35K55, 65P05

1 Introduction

Nonlinear image multiscale analysis is an important task of computer vision. It is related to selective nonlinear filtering, edge detection, enhancement, segmentation and further operations of image processing. With a new development of medical applications, an efficient and robust treating of 3D problems is highly desirable.
The "scaling of the image" is represented by a solution of a nonlinear PDE for which the processed image gives an initial condition. In the last decade such models have been suggested and studied, and in general they are based on degenerate diffusion equations, see for instance [14], [7], [12], [13], [2], [8], [15]. The multiscale approach has been axiomatized, i.e. derived from "first principles", in [1]. There, it was proved in a rigorous way that the majority of image processing operations can be viewed as solutions of second order degenerate parabolic partial differential equation. In some sense, it summarizes the linear scale space theories, started in the eighties by Witkin and Koenderink and a few decades before by Iijima, as well as the ideas of the so-called "morphological school", see [10], [18], [17], [16].
In this paper, we consider the following problem, which is an interesting combination of linear and nonlinear scale space ideas. Let u be the solution of

$$\partial_t b(u) - \nabla(g(|\nabla G_\sigma * u|)\nabla u) = f(u^0 - u) \quad \text{in } Q_T \equiv I \times \Omega, \tag{1.1}$$

$$\partial_\nu u = 0 \quad \text{on } I \times \partial\Omega, \tag{1.2}$$

$$u(0,\cdot) = u^0 \quad \text{in } \Omega, \tag{1.3}$$

* Zentrum für Technomathematik, Universität Bremen, FB 3, Postfach 330440, 28334 Bremen, Germany
†Department of Mathematics, Slovak University of Technology, Radlinského 11, 813 68 Bratislava, Slovakia

where $\Omega \subset I\!R^d$, $d = 3$ in our case, is a bounded domain with Lipschitz continuous boundary, $I = [0, T]$ is a scale interval, and

(1.4) g is a Lipschitz continuous function, $g(0) = 1, 0 < g(s) \to 0$ for $s \to \infty$,

(1.5) $G_\sigma \in C^\infty(I\!R^d)$ is a smoothing kernel, $\int_{I\!R^d} G_\sigma(x)dx = 1$,

(1.6) $G_\sigma(x) \to \delta_x$ for $\sigma \to 0$, $\int\limits_{I\!R^d} |\nabla G_\sigma|^2 dx \le C_\sigma$.

$\nabla G_\sigma * u := \int\limits_{I\!R^d} \nabla_x G_\sigma(x - \xi)\tilde{u}(\xi)d\xi$, where $\tilde{u}$ is an extension of u such that

(1.7) $\|\tilde{u}\|_{L^2(I\!R^d)} \le C\|u\|_{L^2(\Omega)}$.

(1.8) b is a strictly increasing continuous function for which

(1.9) $b(0) = 0$, $\Gamma \ge b'(s) \ge \gamma > 0$,

(1.10) f is a Lipschitz continuous, nondecreasing function with Lipschitz constant L, $f(0) = 0$,

(1.11) $u^0 \in L_\infty(\Omega) \cap V, V = W^{1,2}(\Omega)$.

In [6] we have explained the mechanism of selective smoothing process of the model (1.1)–(1.3) in case $b(s) \equiv s$. Such equation has been suggested by Catté, Lions, Morel and Coll and it combines the ideas of linear Gaussian scaling and nonlinear Perona and Malik anisotropic diffusion equation. We have also reported the role of adaptively coarsened 2D finite element computational grids used in the discrete scale steps. In this paper we present a 3D approach to the problem. We use the structure of tetrahedral meshes obtained by the bisection algorithm ([3], [4], [5]), which can be backwardly coarsened in a straightforward way. Using the coarsening criterion as in [6] we remove tetrahedra from the image regions where the gradient of the image intensity function is small. A "precoarsening" of the initial image is a first tool. The algorithm of coarsening then continues due to the flattening of the image intensity function in the regions outside the edges caused by the smoothing mechanism of (1.1)–(1.3). Moreover, we slightly modify the Catté, Lions, Morel and Coll nonlinear diffusion equation by adding a faster diffusion into those parts of the image which are (a-priori) out of interest of providing image processing operation. Using a small slope of b for such image intensities we speed up the diffusion and thus enhance the grid coarsening. Such effect, together with the opposite, slowing down of the diffusion process depending on the image intensity and/or position in the image, has been suggested and studied in [8], [9]. There, a kind of Jäger-Kačur algorithm is used for the proof of existence of the solution and gives also a numerical approximation. In this paper we consider the nondegenerate case (1.8)–(1.9) in which we use a simpler numerical approximation scheme where all nonlinearities are simply treated from the previous discrete scale step. Thus in each discrete scale step we solve a *linear* elliptic equation by a finite element method with decreasing number of elements due to the coarsening.
In Section 2 we prove that such a method is L_∞-stable in a semi-discrete setting and the same assertion holds true also for the fully discrete scheme using a specific initial triangulation. Since an image can be uniquely represented by a system of its level sets, L_∞-stability is an important criterion for image analysis, e.g., it says that no new level

sets are created in selective smoothing. In Section 3 we discuss in detail the 3D adaptive finite element space discretization and coarsening strategy in 3D. In Section 4 we discuss some computational results with artificial as well as real images.

1 Notation

Let $\Omega \subseteq I\!R^3$ be a bounded domain. Denote by $(u,v) := \int_\Omega u(x)v(x)dx$ the inner product for $u, v \in L^2(\Omega)$. $V := W^{1,2}(\Omega)$ is the Sobolev space of L^2–functions with square integrable weak derivatives.
A *triangulation* $\mathcal{T}$ of Ω is a set of (non–degenerate) tetrahedra with $\bigcup_{T\in\mathcal{T}} T = \bar{\Omega}$.
A triangulation $\mathcal{T}$ is called *conforming* if the intersection of two non–disjoint, non–identical tetrahedra consists either of a common vertex or a common edge. $T \in \mathcal{T}$ is said to have a *non–conforming node*, if there is a vertex P of the triangulation which is not a vertex of T but $P \in T$. A sequence of triangulations $\mathcal{T}_1, \mathcal{T}_2, \ldots$ has the property of *shape regularity* if $\sup_{T\in\mathcal{T}_k, k\in I\!N} \{h_T/\rho(T)\} \leq C$. Here, $h_T := \mathrm{diam}(T)$ and $\rho(T) := \max\{r \mid B_r \subset T\}$ denotes the radius of the largest ball inscribed T.

2 Numerical approximation scheme

In order to solve (1.1)–(1.3) we use the following **semi-implicit linear approximation scheme:**
Let $n \in I\!N, \tau = \frac{T}{n}, 0 < \tau \leq 1/2, t_i = i\tau$ and $\sigma > 0$ be fixed numbers and u^0 be given by (1.3). For $i = 1, \ldots n$, let $u^i \in V$ be the solution of

$$\Big(b'(u^{i-1})(u^i - u^{i-1}), v\Big) + \tau(g(|\nabla G_\sigma * u^{i-1}|)\nabla u^i, \nabla v) = \tau(f(u^0 - u^{i-1}), v), \tag{2.1}$$

for all $v \in V$. These scale–discrete (u^i)'s represent approximations of the image intensity function at the discrete scale instants t_i.

For the scale–discrete u^i's we state the following result.

Theorem 1. *For every $i = 1, ..., n$ there exists a unique solution u^i of (2.1). Moreover, there exists a positive constant C such that*

$$||u^i||_\infty \leq C||u^0||_\infty.$$

The constant C is a nondecreasing function of $1/\gamma, T$ and the Lipschitz constant L of f. If $f \equiv 0$ then $C = 1$.

Proof. Our assertion is clearly true for u^0. Let it hold for u^{i-1}.
Due to (1.6), (1.7) and the Cauchy-Schwarz inequality we derive

$$|\nabla G_\sigma * u^{i-1}| \leq D_\sigma < \infty,$$

and so there exists a constant ν_σ such that

$$g^{i-1} := g(|\nabla G_\sigma * u^{i-1}|) \geq \nu_\sigma > 0. \tag{2.2}$$

Thus, for any fixed σ, by the Lax–Milgram theorem and (1.9) we have existence and uniqueness of $u^i \in V$ which is the solution of (2.1). Moreover $u^i \in L_\infty(\Omega)$, see [11]. Thus the first part of the assertion is proved.
By the above conclusion we know that $v = u^i|u^i|^{p-1} \in V$ and we can use it as a test function in (2.1) for any $p \in I\!N$. Using (1.9) and (1.10) we obtain

$$\int_\Omega b'(u^{i-1})|u^i|^{p+1}dx + \tau \int_\Omega g^{i-1}p|u^i|^{p-1}|\nabla u^i|^2 dx \leq$$

$$\int_\Omega b'(u^{i-1})|u^{i-1}||u^i|^p dx + L\tau \int_\Omega |u^0||u^i|^p dx + \frac{L}{\gamma}\tau \int_\Omega b'(u^{i-1})|u^{i-1}||u^i|^p dx.$$

Let us denote $C_1 = \frac{L}{\gamma}$. Then due to the positivity of the second term on the left hand side we have

$$\int_\Omega b'(u^{i-1})|u^i|^{p+1}dx \leq (1 + C_1\tau) \int_\Omega b'(u^{i-1})|u^{i-1}||u^i|^p dx + L\tau \int_\Omega |u^0||u^i|^p dx. \tag{2.3}$$

Now we use Young's inequality in the form

$$ab \leq \frac{1}{p+1}a^{p+1} + \frac{p}{p+1}b^{\frac{p+1}{p}}$$

in the last term of (2.3) with $a = \varepsilon|u^0|$, $b = \frac{1}{\varepsilon}|u^i|^p$. This together with (1.9) gives us

$$\int_\Omega b'(u^{i-1})|u^i|^{p+1}dx \leq (1 + C_1\tau) \int_\Omega b'(u^{i-1})|u^{i-1}||u^i|^p dx + L\tau\frac{\varepsilon^{p+1}}{p+1} \int_\Omega |u^0|^{p+1}dx +$$

$$+C_1\tau\frac{p}{p+1}\frac{1}{\varepsilon^{\frac{p+1}{p}}} \int_\Omega b'(u^{i-1})|u^i|^{p+1}dx.$$

Let us take $\varepsilon = \left(C_1\frac{p}{p+1}\right)^{\frac{p}{p+1}}$. Subtracting the last term we get

$$(1-\tau)\int_\Omega b'(u^{i-1})|u^i|^{p+1}dx \leq (1 + C_1\tau) \int_\Omega b'(u^{i-1})|u^{i-1}||u^i|^p dx + L\tau\frac{\varepsilon^{p+1}}{p+1} \int_\Omega |u^0|^{p+1}dx.$$

Since for $\tau \leq \frac{1}{2}$ we have $\frac{1}{1-\tau} \leq (1 + 2\tau)$ we obtain

$$\int_\Omega b'(u^{i-1})|u^i|^{p+1}dx \leq (1 + C_1\tau)(1 + 2\tau) \int_\Omega b'(u^{i-1})|u^{i-1}||u^i|^p dx +$$

$$+(1 + 2\tau)L\tau\frac{\varepsilon^{p+1}}{p+1} \int_\Omega |u^0|^{p+1}dx.$$

Let us use Young's inequality with $a = (1 + C_1\tau)(1 + 2\tau)|u^{i-1}|$, $b = |u^i|^p$ in the first term on the right hand side and get

$$\int_\Omega b'(u^{i-1})|u^i|^{p+1}dx \leq \frac{(1 + C_1\tau)^{p+1}(1 + 2\tau)^{p+1}}{p+1} \int_\Omega b'(u^{i-1})|u^{i-1}|^{p+1}dx +$$

$$+\frac{p}{p+1}\int_\Omega b'(u^{i-1})|u^i|^{p+1}dx + (1 + 2\tau)L\tau\frac{\varepsilon^{p+1}}{p+1} \int_\Omega |u^0|^{p+1}dx.$$

Multiplying the previous inequality by $p+1$, subtracting the second term on the right hand side and using (1.9) we obtain the recurrent relation

$$\int_\Omega |u^i|^{p+1}dx \le (1+C_1\tau)^{p+1}(1+2\tau)^{p+1}\frac{\Gamma}{\gamma}\int_\Omega |u^{i-1}|^{p+1}dx + (1+2\tau)C_1\tau\varepsilon^{p+1}\int_\Omega |u^0|^{p+1}dx.$$

Then by the induction we get

$$\int_\Omega |u^i|^{p+1}dx \le (1+C_1\tau)^{i(p+1)}(1+2\tau)^{i(p+1)}\left(\frac{\Gamma}{\gamma}\right)^i(1+(1+2\tau)C_1T\varepsilon^{p+1})\int_\Omega |u^0|^{p+1}dx.$$

Taking the $(p+1)$-th root in the previous inequality and sending $p\to\infty$ (i is fixed and finite) we derive

$$||u^i||_\infty \le e^{(2+C_1)T}(1+C_1)||u^0||_\infty \le C||u^0||_\infty,$$

since $(1+x)^i \le e^{ix}$. Here, the constant C depends on T, $1/\gamma$ and the Lipschitz constant L of f. Provided $f(s)\equiv 0$, a review of the arguments used above shows $C=1$ without any restriction on the time step τ. ∎

The image may be understood as a piecewise linear function interpolating the given discrete values of the image intensity function. The centers of the image voxels then correspond in a natural way to the nodes of a finite element grid. Such an approach is natural for linear finite element discretization, see below.
As the smoothing kernel in (1.1) we use the Gauss function

$$G_\sigma(x) = \frac{1}{(2\sqrt{\pi\sigma})^d}e^{-\frac{|x|^2}{4\sigma}} \tag{2.4}$$

with a given positive σ. In that case the term $\nabla G_\sigma * u^{i-1}$ in (2.1) represents the gradient of the solution at time σ of the heat equation in $\mathbb{R}^3$ with u^{i-1} as initial datum. Using that idea, we replace the convolution term in (2.1) by solving implicitly the linear heat equation for just one discretization step with length σ. Thus, we end up with the following system of equations, semi–implicit in scale:

$$(b'(u^{i-1})u^i, v) + \tau(g(|\nabla u^c|)\nabla u^i, \nabla v) = (b'(u^{i-1})u^{i-1} + \tau f(u^0 - u^{i-1}), v) \tag{2.5}$$

where $u^c \in V$ replaces the convolution $G_\sigma * u^{i-1}$ and is the solution of the problem

$$(u^c, v) + \sigma(\nabla u^c, \nabla v) = (u^{i-1}, v). \tag{2.6}$$

The weak identities (2.5)–(2.6) are starting points to derive a fully discrete semi–implicit finite element discretization of (1.1)–(1.3). To that goal the variational identities (2.5)–(2.6) are projected to finite dimensional subspaces consisting of piecewise linear finite elements $V_h \subset V$, $V_h = V_h(\mathcal{T}_i) := \{v \in C^0(\bar\Omega) | v_{|T} \in \mathcal{P}_1 \text{ for all } T \in \mathcal{T}_i\}$, where $\mathcal{T}_i$ is a conformal triangulation of $\Omega \subseteq \mathbb{R}^3$ at the i–th discrete scale step. By introducing the Lagrangian bases of hat functions $\varphi_j \in V_h(\mathcal{T}_i)$, determined by $\varphi_j(x_k) = \delta_{j,k}$ for all vertices x_k, $k = 1, \dots N_i$ of $\mathcal{T}_i$, N the number of vertices, a function $v_h \in V_h$ is given by $v_h = \sum_{k=1}^N v_k\varphi_k = \sum_{k=1}^N v(x_k)\varphi_k$.

For each discrete scale instant $i = 1, \dots n$ we are looking for a function $u_h^i \in V_h(\mathcal{T}_i)$ fulfilling

$$(2.7) \qquad \begin{aligned}(b'(u_h^{i-1}); u_h^i, v_h)_h + \tau(g(|\nabla u_h^c|)\nabla u_h^i, \nabla v_h) &= (b'(u_h^{i-1}); u_h^{i-1}, v_h)_h \\ &\quad + \tau(f(u_0 - u_h^{i-1}), v_h)\end{aligned}$$

for all $v_h \in V_h(\mathcal{T}_i)$ where $u_h^c \in V_h(\mathcal{T}_i)$ is the solution of

$$(2.8) \qquad (\mathbb{1}; u_h^c, v_h)_h + \sigma(\nabla u_h^c, \nabla v_h) = (\mathbb{1}; u_h^{i-1}, v_h)_h \quad \forall v_h \in V_h(\mathcal{T}_i),$$

where $(w; u_h, v_h)_h$ is the lumped L^2 inner product, defined by

$$(w; u_h, v_h)_h := \sum_k w(x_k) u_h(x_k) v_h(x_k) \int_\Omega \varphi_k.$$

Using the above bases representation (2.7)–(2.8) may be written in the form

$$\begin{aligned}\sum_{k=1}^N \Big\{(b'(u_h^{i-1})\varphi_k, \varphi_j)_h + \tau(g(|\nabla u_h^c|)\nabla\varphi_k, \nabla\varphi_j)\Big\} u_k^i &= (b'(u_h^{i-1})u_h^{i-1}, \varphi_j)_h \\ &\quad + \tau(f(u_0 - u_h^{i-1}), \varphi_j)\end{aligned}$$

and

$$\sum_{k=1}^N \Big\{(\varphi_k, \varphi_j) \; + \; \sigma(\nabla\varphi_k, \nabla\varphi_j)\Big\} u_k^c = (u_h^{i-1}, \varphi_j)$$

for all $j = 1, \dots N$.
Thus solving (2.7)–(2.8) means inverting two linear systems with matrices

$$\mathbf{M}(b'(u_h^{i-1})) + \tau\mathbf{A}(g(|\nabla u_h^c|)),$$

$$\mathbf{M}(\mathbb{1}) + \sigma\mathbf{A}(\mathbb{1}),$$

with $\mathbf{M}_{j,k}(w) = (w; \varphi_k, \varphi_j)_h$ the lumped mass matrix and $\mathbf{A}(w)_{j,k} = (w\nabla\varphi_k, \nabla\varphi_j)$ the stiffness matrix.

3 Multiscale image coarsening

As mentioned above, we use a coarsening strategy for the finite element meshes to increase the effectiveness of the procedure. Since the image is being smoothed as scale time evolves and we do not expect a movement of contour lines, coarsening is an appropriate way to decrease the number of unknowns.
To be more precise we proceed as follows. We generate a triangulation $\tilde{\mathcal{T}}_0$ by refining a coarse grid $\mathcal{T}^0$, the so called *macro triangulation*. We choose the *bisection method*, which allows for coarsening quite easily and was introduced for the 3D case in [3]. This refinement procedure generates a sequence $\mathcal{T}^0, \mathcal{T}^1, \mathcal{T}^2, \dots$ of finer and finer meshes until the desired (initial) mesh width is reached.
After this initialization we perform some steps of *precoarsening* to $\tilde{\mathcal{T}}_0$ resulting in the starting triangulation $\mathcal{T}_0$. During time–scale evolution, in every time–step coarsening again is used to reduce the number of unknowns according to a certain coarsening criterion, see below.
We briefly recall the bisection method, for further details see [3]:

3.1 Refinement by bisection

Consider a tetrahedron $T \in \mathcal{T}^0$, which has been cut open along the three edges which meet at vertex P_4 and unfolded:

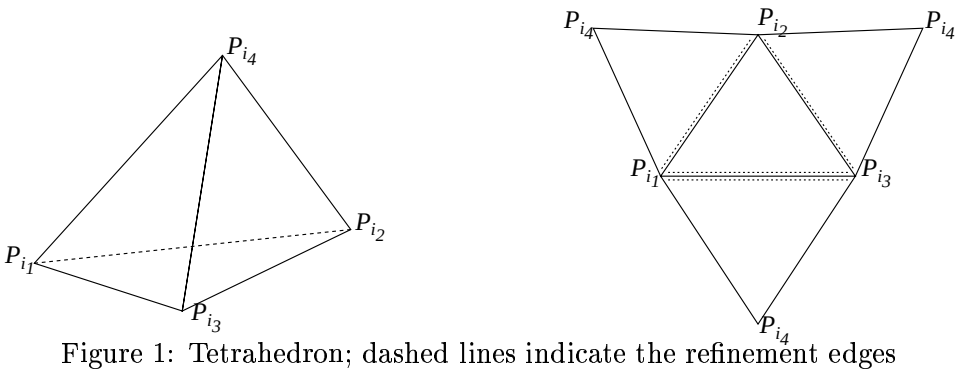

Figure 1: Tetrahedron; dashed lines indicate the refinement edges

With each of the four triangular faces of T we associate a *refinement edge* (one example is shown in Figure 1). We make the following assumptions:

(A1) For each tetrahedron there is at least one common refinement edge for two different faces of the tetrahedron adjacent to this edge ($\overline{P_{i_1}P_{i_3}}$ in Figure 1). We call such an edge a *global refinement edge* of the tetrahedron.

(A2) If T_1, T_2 are two tetrahedra with $T_1 \cap T_2 = S$ and S is a triangle, then the refinement edge of S with respect to T_1 and the refinement edge of S with respect to T_2 is the same.

Note that assumptions (A1) and (A2) can be fulfilled for an arbitrary conforming triangulation: There is an ordering of the edges of a triangulation (for instance in terms of their lengths). Choose the refinement edge of a triangular face as the one with highest index corresponding to this ordering. Then (A1) and (A2) are fulfilled.
Let us first consider the split of a single tetrahedron:
A single tetrahedron is bisected by cutting through the midpoint of the global refinement edge to the opposite vertices, thus introducing the midpoint as a new node P_{new}. We get two new tetrahedra:

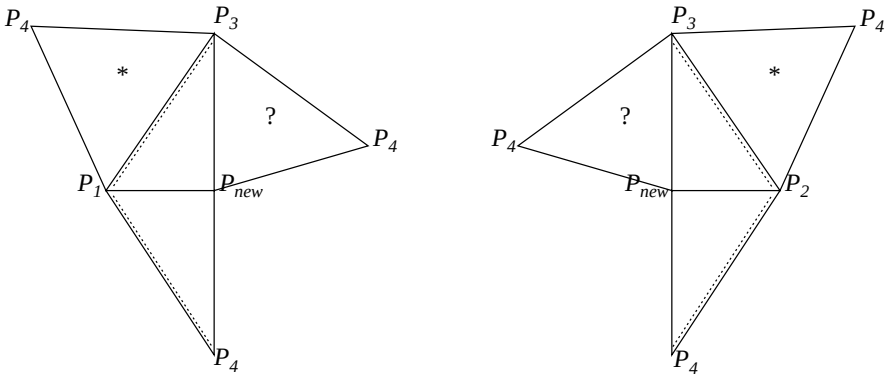

Figure 2: Bisection of a single tet.

The refinement edges of the bisected triangles are chosen as indicated by Figure 2. Here, $*$ indicates an arbitrary position of the refinement edge which is not affected by the split. The question then is, how to choose the refinement edge for the new triangle $P_{new}P_4P_3$. One requirement is of course the condition that both new tetrahedra must have again a global refinement edge.
In [3] it is outlined how to choose this refinement edge properly. The above procedure is the atomic operation to split a single element. For the global situation the following algorithm is used.

Bisection algorithm:
Let $\mathcal{T}^k$ be a given triangulation, either $k = 0$ or $\mathcal{T}^k$ being a refinement of $\mathcal{T}^{k-1}$. Let $\Sigma^+ \subseteq \mathcal{T}^k$ be a set of tetrahedra to be divided.

while $\Sigma^+ \neq \emptyset$ **do**

`bisect all` $T \in \Sigma^+$ `as described above, obtain the intermediate triangulation` $\hat{\mathcal{T}}^k$ `(possibly non-conforming)`

`let now` Σ^+ `be the set of those tetrahedra with a non-conforming node.`

endwhile
$\mathcal{T}^{k+1} := \hat{\mathcal{T}}^k$

In [3] the following is shown:
Theorem 2.: Let the conforming triangulation $\mathcal{T}^k$ fulfill assumptions (A1) and (A2). Then the above algorithm stops in a finite number of steps and $\mathcal{T}^{k+1}$ is conforming. The sequence $\mathcal{T}^0, \mathcal{T}^1, \mathcal{T}^2, \ldots$ is shape regular.

Remark: Let Ω be a cube (which is quite natural in image processing). Then starting from a natural subdivision into 6 tetrahedra of the cube as the macro triangulation and using the bisection method to generate the triangulations, it is simple to show that the fully discrete equations fulfil a discrete maximum principle in the case $f \equiv 0$, see for instance [19]. Here, we made use of the fact that $\nabla u^c_{|T}$ is constant for every tetrahedron T. Thus we get an estimate

$$||u_h^i|_\infty \leq ||u_h^0|_\infty$$

for all $i = 1, \ldots n$.

3.2 Local coarsening

We choose the bisection method to generate the starting triangulation $\mathcal{T}_0$ because a triangulation which was derived by a successive application of bisection steps can be derefined very easily. We make the following definitions:
Definition:

i.) A tet $T \in \mathcal{T}$ has level l if T was obtained after l refinement steps.

ii.) A tet T is said to have *locally finest level* if the levels of all neighbors are less than or equal to the level of T.

iii.) Let $T \in \mathcal{T}$ and let T' be the father of T. A vertex P of T which was inserted while bisecting T' is called the *coarsening node* of T.

iv.) Let K be an edge of the triangulation $\mathcal{T}$ and K' the "father"–edge of K with midpoint Q. Set $M := \{T \in \mathcal{T} | T \cap K' \neq \emptyset\}$. If Q is the coarsening node for all $T \in M$ then M is called a *resolvable patch.*

Figure 3 shows a resolvable patch and the coarsened patch.

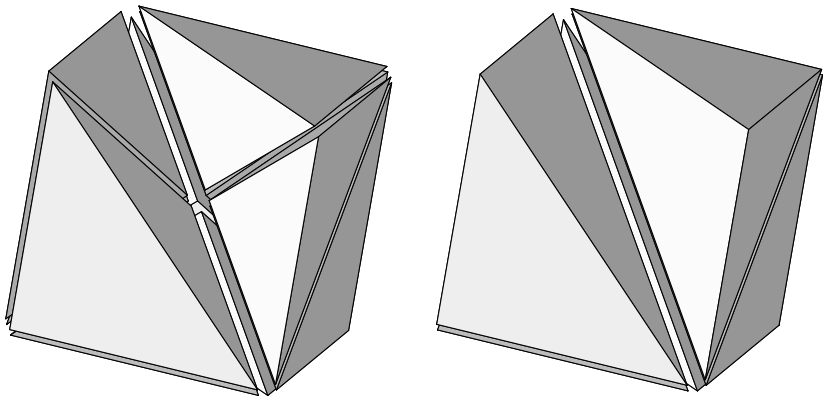

Figure 3: Resolvable patch and coarsened patch

If M is a resolvable patch, then all $T \in M$ can be coarsened without interfering with $T' \in \mathcal{T}$ outside of M. Therefore resolvable patches are the configurations which we allow to be coarsened. This guarantees that the coarsening process stays local.

We may write the coarsening algorithm in the following form:

Coarsening algorithm:
Let $\mathcal{T}^i$ be a triangulation obtained by refinement and coarsening steps. Let $\Sigma^- \subset \mathcal{T}^i$ be the set of tetrahedra to be derefined. Then one coarsening step consists of:

```
for each T ∈ Σ⁻ do
    if T belongs to a resolvable patch M then
        if T' ∈ Σ⁻ for all T' ∈ M then
            derefine M, see Figure 3
        endif
    endif
enddo
```

Since we only derefine resolvable patches the question arises whether there are "enough" resolvable patches in an arbitrary triangulation. In [5] it is shown that at least for so–called "standard triangulations" the following holds: All tetrahedra of locally finest levels belong to resolvable patches. This means that using the above algorithm a total derefinement of a triangulation is possible.

3.3 Coarsening criterion and adaptive method

As the local behavior of ∇u determines the evolution process and is an indicator for edges, the coarsening criterion is based on this value. More precisely, let $\epsilon > 0$ be a given tolerance. For i a time–scale step and u_h^i the corresponding numerical solution on the grid $\mathcal{T}_i$ we allow all tetrahedra $T \in \mathcal{T}_i$ to be coarsened, if

$$h_T |\nabla u_h^i| \leq \epsilon \quad \text{on } T. \tag{3.1}$$

Note that since u_h^i is piecewise linear, ∇u_h^i is constant on each tetrahedron.
Thus we have the following adaptive scheme to approximate (1.1)–(1.3):

Let $\mathcal{T}_0, u_0$ be given.

for $i = 1, 2, \ldots n$ **do**
`set up the matrix` $\mathbf{M} + \sigma \mathbf{A}(\mathbb{1})$
`compute` $u_h^c \in V_h(\mathcal{T}_i)$ `solving (2.8)`
`set up the matrix` $\mathbf{M} + \tau \mathbf{A}(g(|\nabla u_h^c|))$
`compute` $u_h^i \in V_h(\mathcal{T}_i)$ `solving (2.7)`
`define` $\Sigma^- := \{T \in \mathcal{T}_i \mid h_T |\nabla u_h^i| \leq \epsilon$ `on` $T\}$
`derefine` $\mathcal{T}_i$ `according to` Σ^- `to obtain` $\mathcal{T}_{i+1}$
enddo

4 Numerical experiments

In this Section we present two numerical examples computed by the scheme (2.7)–(2.8) using the 3D coarsening strategy. In the computations we used the following definition for g:

$$g(s) = \frac{1}{1 + 5s^2}.$$

In the first example we added noise to an artificial image containing the object visualized in Figure 4. In Figure 5 we plot successive filtering of the initially noisy image until the desired object is extracted. In Figures 6 and 7 we plot the results of scaling together with a cut of the computational tetrahedral grid in order to illustrate the local coarsening. IN this example we took $b(s) = s$. Table 1 shows the decrease in the number of degrees of freedom due to coarsening. Note that the difference from the 0th to the 1st time step results from the precoarsening.
Next, we have applied our method to a real image representing an in vivo acquired 3D echo-cardiography. The acquisition represents a certain time instant of the cardiac cycle of a real patient. In Figure 8 the isosurface corresponding to the interface between the cardiac muscle and blood is visualized using an original echo-image (top left) and after

time step	0	1	2	3	4	5	6
♯ unknowns	274625	273948	270789	256715	228774	191386	138738

time step	7	8	9	10
♯ unknowns	81049	47245	30929	19475

Table 1: Decrease of unknowns, example 1

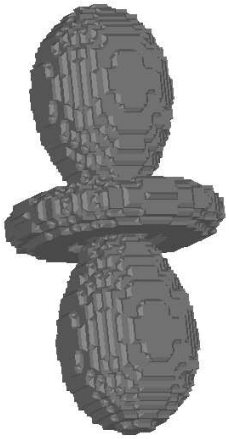

Figure 4: Original artificial image without noise.

processing by our algorithm. We took advantage of the fact that the grey value describing this interface is known by setting

$$b(s) = \begin{cases} s & \text{for} \quad s \leq s^*, \\ 10^{-3}s + s^* & \text{for} \quad s > s^*, \end{cases}$$

where s^* is sufficiently larger than the level of this isosurface.

time step	0	1	2	3	4	5	6	7	8
♯ unknowns	274625	141621	122273	104334	94253	88066	83392	79221	75392

Table 2: Decrease of unknowns, example 2

Acknowledgment We would like to thank Claudio Lamberti and Alessandro Sarti from the University of Bologna for providing the 3D echocardiographic data.

References

[1] L. Alvarez, F. Guichard, P.L. Lions, J.M. Morel: *Axioms and Fundamental Equations of Image Processing.* Archive for Rat. Mech. Anal., vol.123, pp. 200-257 (1993)

[2] L. Alvarez, P.L. Lions, J.M. Morel : *Image selective smoothing and edge detection by nonlinear diffusion II.* SIAM J.Numer.Anal., vol. 29, pp. 845-866 (1992)

[3] E. Bänsch: *Local Mesh Refinement in 2 and 3 Dimensions.* IMPACT of Computing in Science and Engineering, no. 3, 181–191 (1991)

[4] E. Bänsch: *Adaptive Finite–Element Techniques for Navier–Stokes Equations and other Transient Problems.* In: Adaptive Finite and Boundary Elements, Computational Mechanics Publications and Elsevier (1993)

[5] E. Bänsch: *Mesh refinement in two and three dimensions.* In: INRIA course "Calcul d'erreur a posteriori et adaptation de maillage", Rocquencourt (France) 9/1995

[6] E. Bänsch, K.Mikula: *A coarsening finite element strategy in image selective smoothing.* Computing and Visualization in Science 1, pp. 53-61 (1997)

[7] F. Catté, P.L. Lions, J.M. Morel, T. Coll: *Image selective smoothing and edge detection by nonlinear diffusion.* SIAM J. Numer. Anal., vol. 129, pp. 182-193 (1992)

[8] J. Kačur, K. Mikula: *Slow and fast diffusion effects in image processing - Approximation schemes and numerical experiments.* Preprint IWR 96-26, University of Heidelberg (1996)

[9] J. Kačur, K. Mikula: *Slowed anisotropic diffusion.* Scale-space theory in computer vision (ed. by B.t.H.Romeny et al.), Lecture Notes in Computer Science 1252, pp. 357-360 (1997)

[10] J.J. Koenderink: *The structure of images*, Biol.Cybern., Vol 50, pp. 363-370 (1984)

[11] O.A. Ladyzenskaja, N.N. Uralceva: Linear and Quasilinear elliptic equations, Academic Press (1968)

[12] M. Nitzberg, T. Shiota: *Nonlinear image filtering with edge and corner enhancement.* IEEE Trans. Pattern Anal. Mach. Intel. Vol. 14 (1992) 826-833

[13] S. Osher, L.Rudin: *Feature oriented image enhancement using shock filters*, SIAM J. Numer. Anal. (1990), 919-940

[14] P. Perona, J. Malik: *Scale space and edge detection using anisotropic diffusion.* In Proc. IEEE Computer Society Workshop on Computer Vision (1987)

[15] B.M. ter Haar Romeny (Ed.): *Geometry driven diffusion in computer vision.* Kluwer (1994)

[16] J.Serra: *Image analysis and mathematical morphology.* Academic Press, New York (1982)

[17] J. Weickert, S. Ishikawa, A. Imiya: *Scale space has been discovered in Japan*, Technical report DIKU-TR-97/18, Dept. of Comp. Sci., Univ. of Copenhagen (1997)

[18] A.P. Witkin: *Scale-space filtering.* Proc. Eight Int. Conference on Artificial Intelligence, Vol 2, pp. 1019-1022 (1983)

[19] J. Xu, L. Zikatanov: *A monotone finite element scheme for convection-diffusion equations.* Math. Comput. 68, No.228, 1429-1446 (1999)

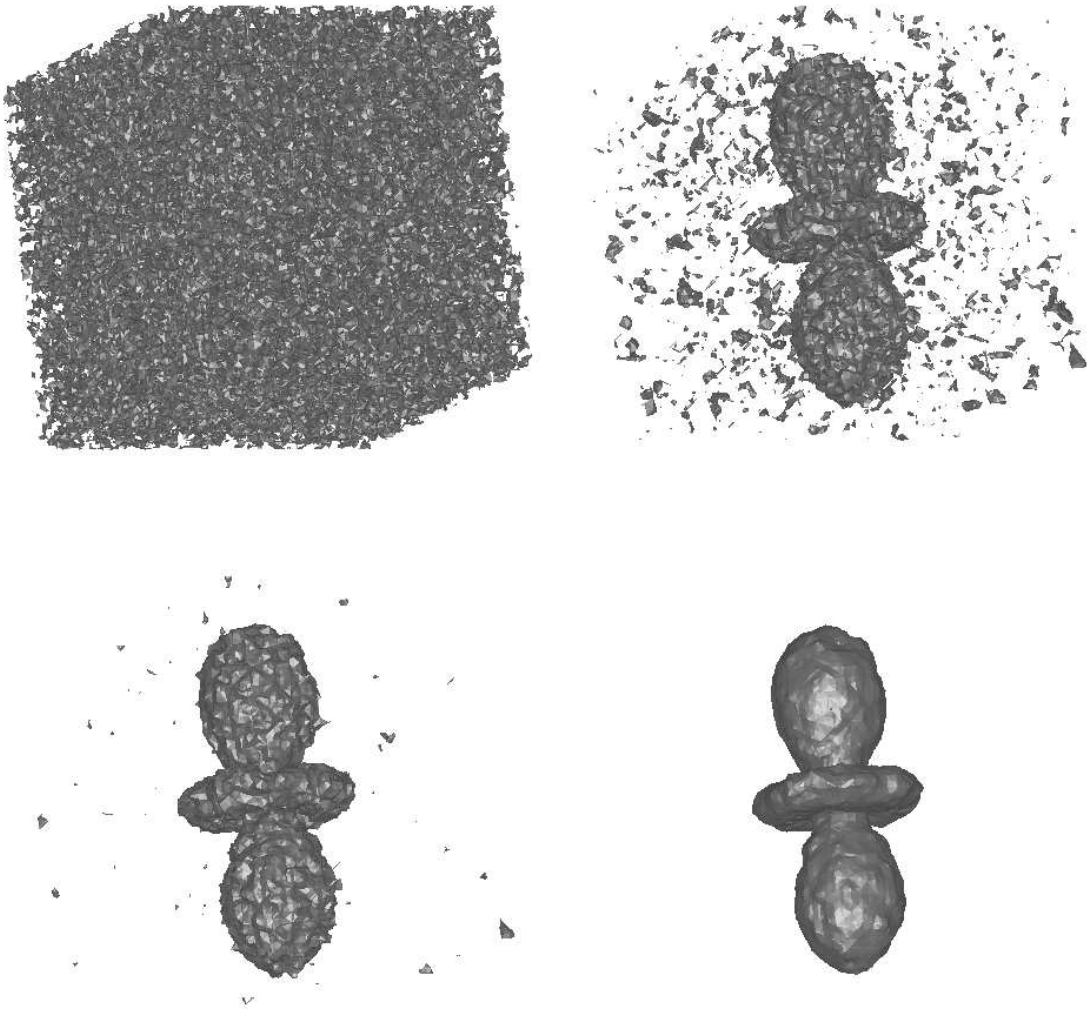

Figure 5: Smoothing of the artificial image.

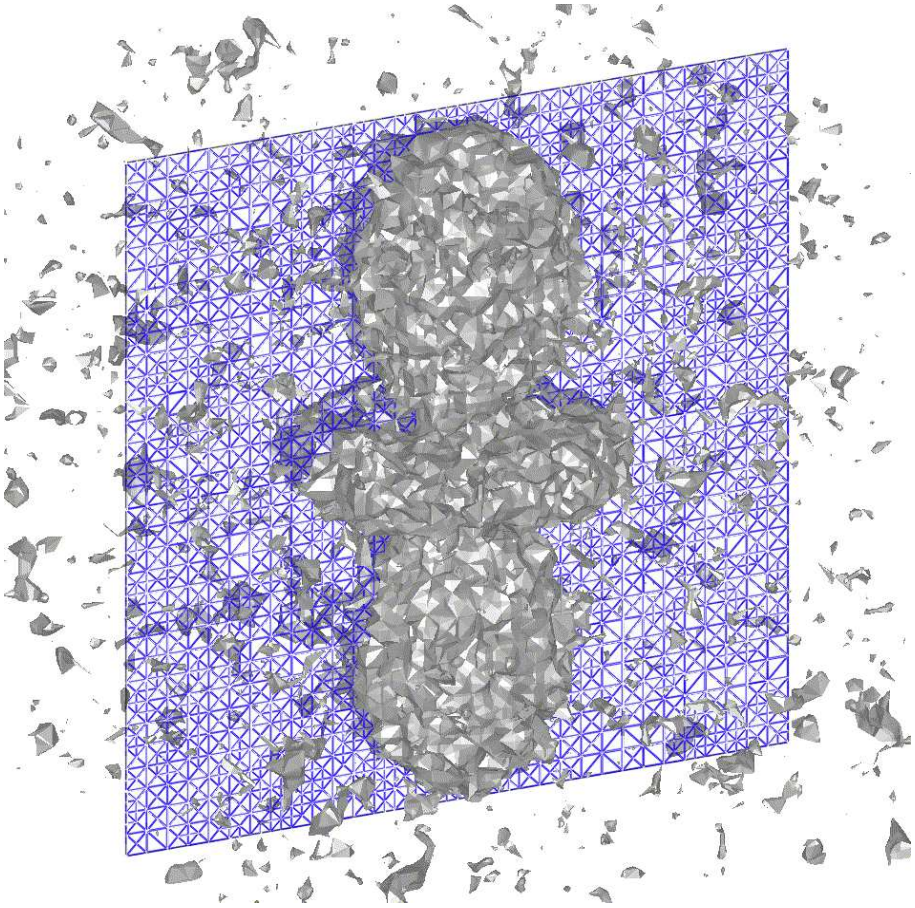

Figure 6: Level surface and computational grid at the 4th scale step.

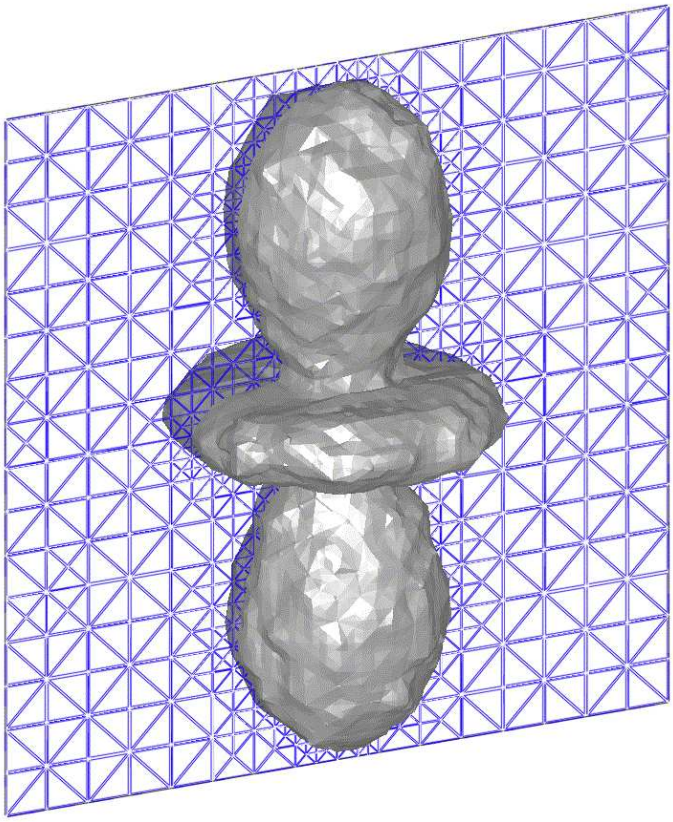

Figure 7: Level surface and computational grid at the 10th scale step.

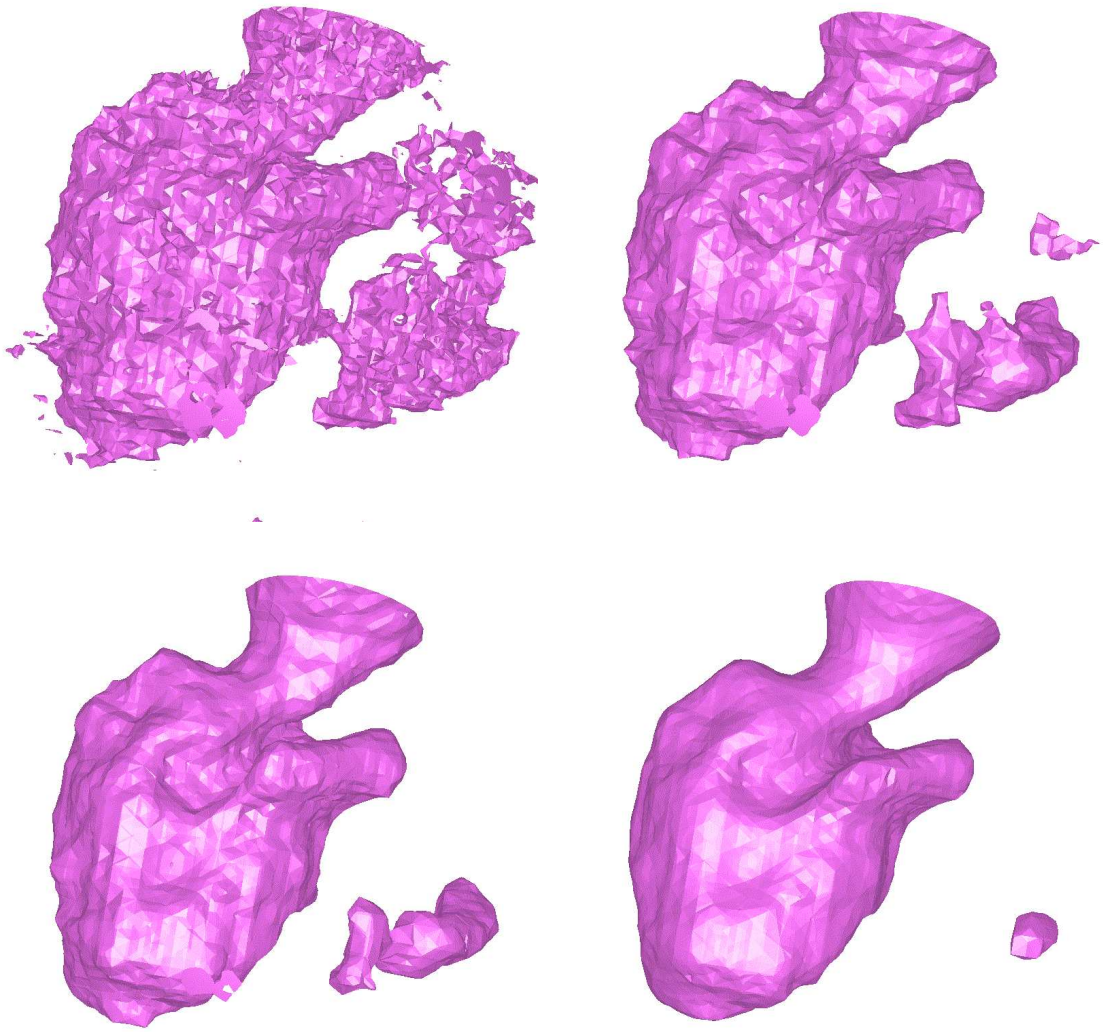

Figure 8: Smoothing of the human left ventricle. Visualization of the corresponding level surfaces at the 0th, 2nd, 4th and 8th scale steps respectively.

Berichte aus der Technomathematik ISSN 1435-7968

`http://www.math.uni-bremen.de/zetem/berichte.html`

— Vertrieb durch den Autor —

Reports **Stand: 13. Dezember 1999**

98–01. Peter Benner, Heike Faßbender:
An Implicitly Restarted Symplectic Lanczos Method for the Symplectic Eigenvalue Problem, Juli 1998.

98–02. Heike Faßbender:
Sliding Window Schemes for Discrete Least-Squares Approximation by Trigonometric Polynomials, Juli 1998.

98–03. Peter Benner, Maribel Castillo, Enrique S. Quintana-Ortí:
Parallel Partial Stabilizing Algorithms for Large Linear Control Systems, Juli 1998.

98–04. Peter Benner:
Computational Methods for Linear–Quadratic Optimization, August 1998.

98–05. Peter Benner, Ralph Byers, Enrique S. Quintana-Ortí, Gregorio Quintana-Ortí:
Solving Algebraic Riccati Equations on Parallel Computers Using Newton's Method with Exact Line Search, August 1998.

98–06. Lars Grüne, Fabian Wirth:
On the rate of convergence of infinite horizon discounted optimal value functions, November 1998.

98–07. Peter Benner, Volker Mehrmann, Hongguo Xu:
A Note on the Numerical Solution of Complex Hamiltonian and Skew-Hamiltonian Eigenvalue Problems, November 1998.

98–08. Eberhard Bänsch, Burkhard Höhn:
Numerical simulation of a silicon floating zone with a free capillary surface, Dezember 1998.

99–01. Heike Faßbender:
The Parameterized SR Algorithm for Symplectic (Butterfly) Matrices, Februar 1999.

99–02. Heike Faßbender:
Error Analysis of the symplectic Lanczos Method for the symplectic Eigenvalue Problem, März 1999.

99–03. Eberhard Bänsch, Alfred Schmidt:
Simulation of dendritic crystal growth with thermal convection, März 1999.

99–04. Eberhard Bänsch:
Finite element discretization of the Navier-Stokes equations with a free capillary surface, März 1999.

99–05. Peter Benner:
Mathematik in der Berufspraxis, Juli 1999.

99–06. Andrew D.B. Paice, Fabian R. Wirth:
Robustness of nonlinear systems and their domains of attraction, August 1999.

99–07. Peter Benner, Enrique S. Quintana-Ortí, Gregorio Quintana-Ortí:
Balanced Truncation Model Reduction of Large-Scale Dense Systems on Parallel Computers, September 1999.

99–08. Ronald Stöver:
Collocation methods for solving linear differential-algebraic boundary value problems, September 1999.

99–09. Huseyin Akcay:
Modelling with Orthonormal Basis Functions, September 1999.

99–10. Heike Faßbender, D. Steven Mackey, Niloufer Mackey:
Hamilton and Jacobi come full circle: Jacobi algorithms for structured Hamiltonian eigenproblems, Oktober 1999.

99–11. Peter Benner, Vincente Hernández, Antonio Pastor:
On the Kleinman Iteration for Nonstabilizable System, Oktober 1999.

99–12. Peter Benner, Heike Faßbender:
A Hybrid Method for the Numerical Solution of Discrete-Time Algebraic Riccati Equations, November 1999.

99–13. Peter Benner, Enrique S. Quintana-Ortí, Gregorio Quintana-Ortí:
Numerical Solution of Schur Stable Linear Matrix Equations on Multicomputers, November 1999.

99–14 Eberhard Bänsch, Karol Mikula:
Adaptivity in 3D Image Processing, Dezember 1999.